Supporting Information

Simple Te-Thermal Converting 2H to 1T@2H MoS_2 Homojunctions with Enhanced Supercapacitor Performance

Weihao Li[†⊥], Yongli Shen[†⊥], Xiong Xiao[†], Cuihua An[†,*], Guijuan Wei[†], Yaqian Wang[†], Jiayang Wang[†,‡], Yue Wu[‡*], and Changhua An[†,*]

[†]Tianjin Key Laboratory of Organic Solar Cells and Photochemical Conversion, School of Chemistry and Chemical Engineering and Tianjin Key Laboratory of Advanced Functional Porous Materials, Institute of New Energy Materials & Low-Carbon Technologies, Tianjin University of Technology, Tianjin 300384, P. R. China

[‡]Department of Chemical and Biological Engineering, Iowa State University, Ames, Iowa 50011, United States

*Corresponding Author:

Email: ancuihua@tjut.edu.cn; yuewu@iastate.edu; anch@tjut.edu.cn

EXPERIMENTAL PROCEDURES

Synthesis of 2H-MoS_2 nanosheets, and Te doped 1T@2H MoS_2 homojunctions

Hexaammonium heptamolybdate terahydrate ($(NH_4)_6Mo_7O_{24}\cdot 4H_2O$), Thiourea and Te powder (~100 mesh, 99.99%) were purchased from Sinopharm Chemical Regent and Aladdin, respectively. All the chemicals were used as received without further purification. 0.25 mmol of $(NH_4)_6Mo_7O_{24}\cdot 4H_2O$ and 3.5 mmol of CH_4N_2S were dissolved in 8.75 mL of deionized water under magnetically stirring for 10 min. The above mixture was transferred into a 10 mL Teflon-lined autoclave and heated in an electric oven at 220 ℃ for 18 h. Then the autoclave was cooled to room temperature naturally, and the product was collected by centrifugation. Finally, black 2H-MoS_2 nanosheets was rinsed with deionized water and ethanol several times, and dried in vacuum at 60 ℃ overnight.

The as-prepared 2H-MoS_2 and Te powder at a molar ratio of 1:2 were ground and transferred into a tube furnace. The furnace was heated to 700 ℃ at a rate 5 ℃/min under 10% H_2/Ar atmosphere. After the reaction was maintained at that temperature for 8 h, a grey product was collected and treated as above.

Characterizations

Powder X-ray diffraction (XRD) was performed using an Ultima IV X-diffractometer with a Cu *Kα* radiation source (λ = 0.15406 nm). X-ray photoelectronic spectra were obtained from an ESCALAB250Xi with an Al *Kα* radiation source (*hv* = 0.1486.6 eV). The morphologies and microstructures of the 2H-MoS_2 and Te doped 1T@2H MoS_2 nanosheets were characterized by scanning electron microscopy (SEM, ZEISS MERLI) analysis, transmission electron microscopy (TEM, TECNAI G2) and high-resolution transmission electron microscopy (HRTEM, Talos F200 X). Resistance measurement is determined by four probe method.

Electrochemical Performance Evaluation

The electrochemical performance of the as-prepare 2H-MoS_2 and Te doped 1T@2H MoS_2 electrode was evaluated on a CHI 760E electrochemical workstation (Shanghai Chenhua, China). The working electrode was fabricated according to the following procedure: i) the samples, carbon black and poly(tetrafluoroethylene) binder with a mass ratio of 80: 15: 5 was mixed homogenously; ii) the obtained mixture was pressed onto a nickel foam and dried at 60 ℃ for 12 h. An Hg/HgO electrode and platinum plate (1 cmx1cm) were used as the reference electrode and counter electrode, respectively. The electrolyte was 2 M KOH aqueous solution. Cyclic voltammetry (CV) and galvanostatic charge-discharge (GCD) were measured both in a three-electrode and two-electrode cell. Electrochemical impedance spectroscopy (EIS) measurement was carried out in the frequency range from 0.001 Hz to 100 k Hz at open circuit potential with 5 mV amplitude. The specific capacitance (*C*) was calculated according to the following equation based on GCD curves:

$$C = \frac{Q}{v} = \frac{I\Delta t}{\Delta V m}$$

Where *I* is the constant discharge current (A), $\triangle t$ is the discharge time (s), $\triangle v$ is the potential window (V), and *m* (g) is the mass of the active material, respectively. The energy and power density of the asymmetric supercapacitor device are calculated according to the following equations:

$$E = \frac{\mathrm{C}\Delta\mathrm{V}^2}{2}$$

$$P = \mathrm{E}/\mathrm{t}$$

Where *C* represents the capacitance of asymmetric supercapacitors, $\triangle V$ is the cell voltage, and *t* is the discharge time in GCD curves, respectively. The electrochemical performance of asymmetric supercapacitor was also tested according to CV and GCD curves. The negative electrode was prepared by mixing 95 wt.% of AC and 5 wt.% of polytetrafluoroethylenes, and the Te doped

1T@2H MoS_2 electrode was used as positive electrode. The cathode and anode were made of sample and activated carbon to assemble an asymmetric supercapacitor. The electrochemical performance tests of the asymmetric supercapacitor were carried out in a two-electrode cell at room temperature in 2 M KOH aqueous solution.

Computational Methods

Computational details

All calculations presented in this work were performed using the generalized gradient approximation (GGA)-Perdew, Burke and Ernzerhof (PBE)[1] as implemented in the all-electron DMol3 code.[2, 3] The Heterogeneous junction is modelled using a 4×2√3 supercell 2H and a 4×2√3 supercell 1T-MoS_2. The layer spacing is fixed to 6.4 Å. Double numerical plus polarization (DNP) basis set was used throughout the calculation. The convergence criteria were set to be $1x10^{-5}$ Ha, 0.001 $HaÅ^{-1}$, and 0.005 Å for energy, force, and displacement convergence, respectively. A self-consistent field (SCF) density convergence with a threshold value of $1x10^{-6}$ Ha was specified. K-points were sampled using the 3×3×1 Monkhorst-Pack mesh for this Heterogeneous junction.

All calculations presented in this work are carried out using the generalized gradient approximation (GGA)-Perdew, Burke and Ernzerhof (PBE)[4] as implemented in the all-electron DMol3 code.[5,6] Double numerical plus polarization (DNP) basis set was used throughout the calculation. The convergence criteria were set to be $2x10^{-5}$ Ha, 0.004 $HaÅ^{-1}$, and 0.005 Å for energy, force, and displacement convergence, respectively. A self-consistent field (SCF) density convergence with a threshold value of $1x10^{-5}$ Ha was specified. All electronic property analyses are deal with Multiwfn software, a program for realizing electronic wavefunction analysis.[7] Single point energy calculation using Gaussian09 software[8] also carried out for a $TeMo_3S_{11}H_6$ cluster model which is cut off from the optimized Te doped 1T@2H MoS2 structure and all dangling bonds of S are saturated with H, with the aim of getting wave function file needed for the qualitative analysis electronic characters and Bader charge for it using Multiwfn.

3.2. Computational models

In order to construct the heterojunction structure, two 1T (9.60 Å ×16.63 Å) and 2H (9.50 Å ×16.45 Å) basic structures with similar dimensions have been chosen in this work. All different heterojunction structure with the different 1T@2H ratio is obtained by combining the two basic units. The lattice size in the z-direction is set to 6.2 Å, which is consistent with our experimental results. a $TeMo_3S_{11}H_6$ cluster is cut off from the optimized Te doped 1T@2H MoS_2 structure and all dangling bonds of S are saturated with H (See the supplementary materials for the more details).

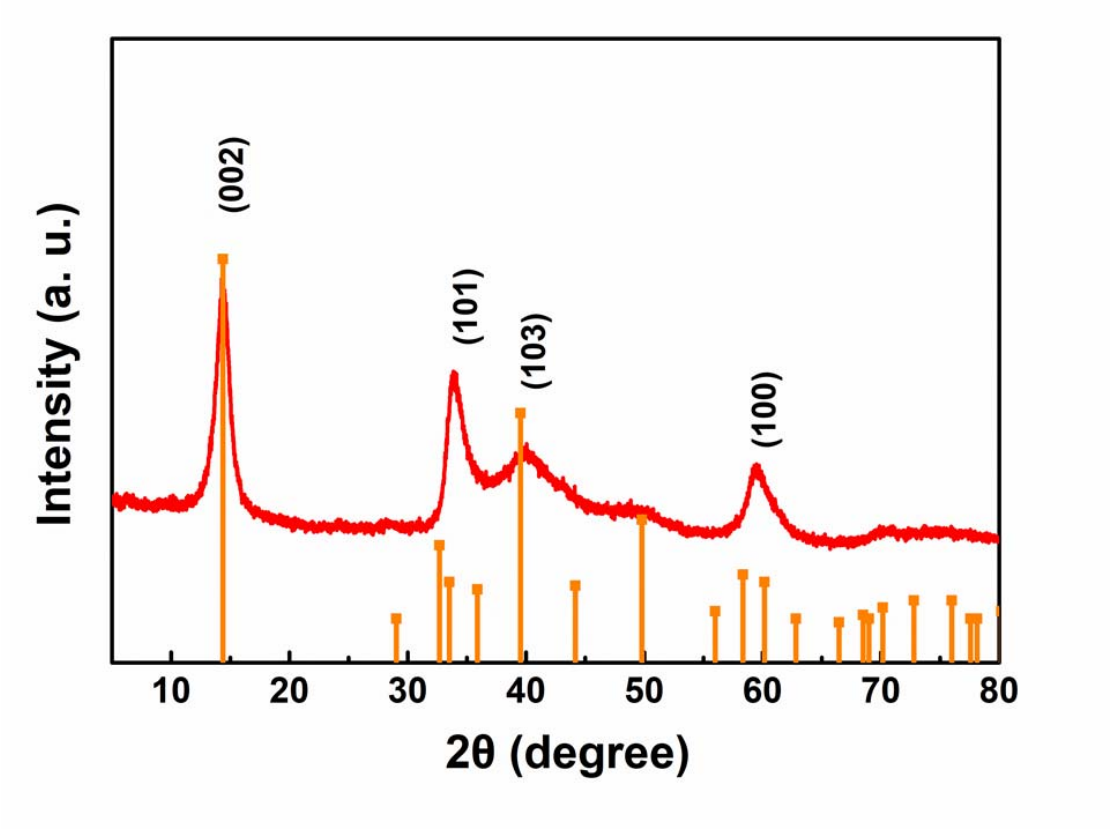

Figure S1. XRD pattern of the annealed 2H-MoS_2 without the presence of Te.

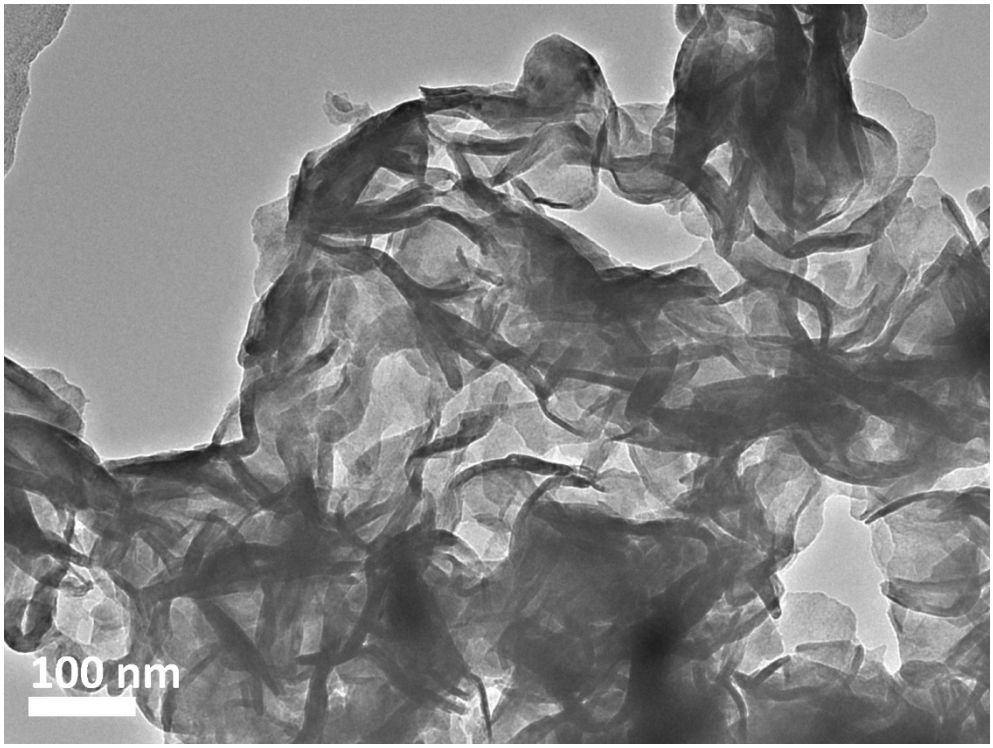

Figure S2. TEM image of the Te doped 1T@2H MoS_2 homojunction nanosheets.

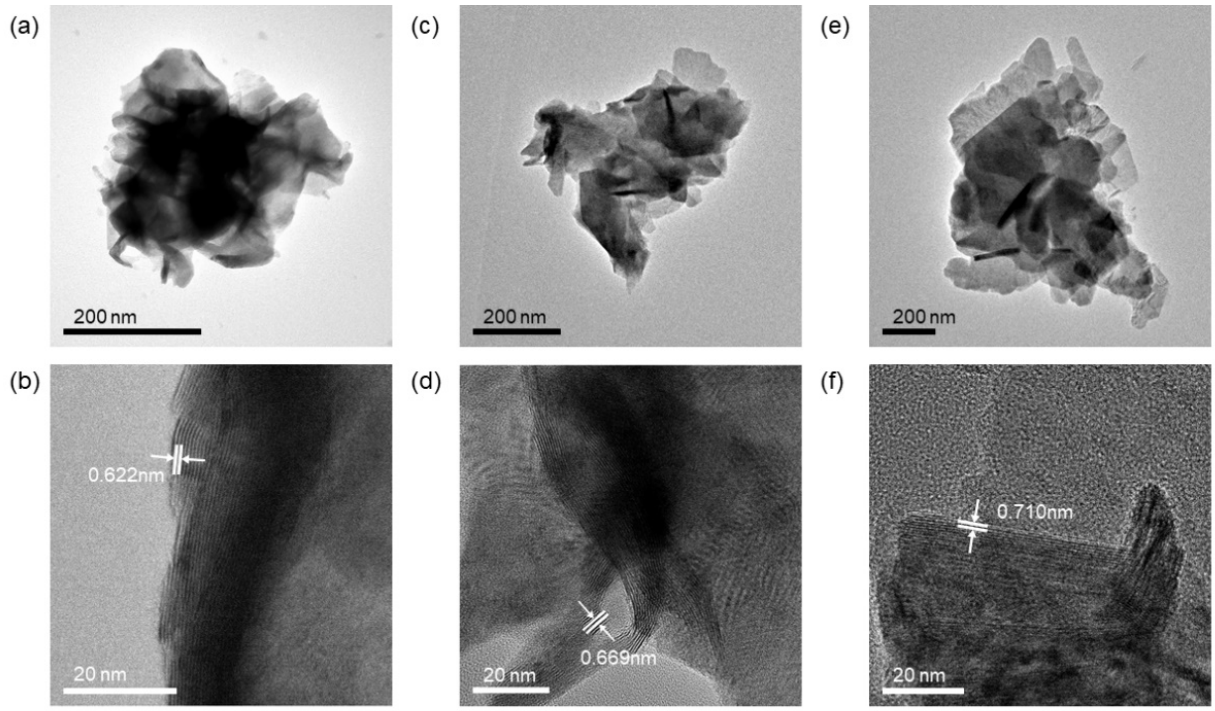

Figure S3. HRTEM images of the Te doped MoS_2 with different molar ratios: (a) and (b) 2H-MoS_2: Te =1:1; (c) and (d) 2H-MoS_2: Te =1:4; (e) and (f) 2H-$MoS_{2:\ Te}$ =1:6.

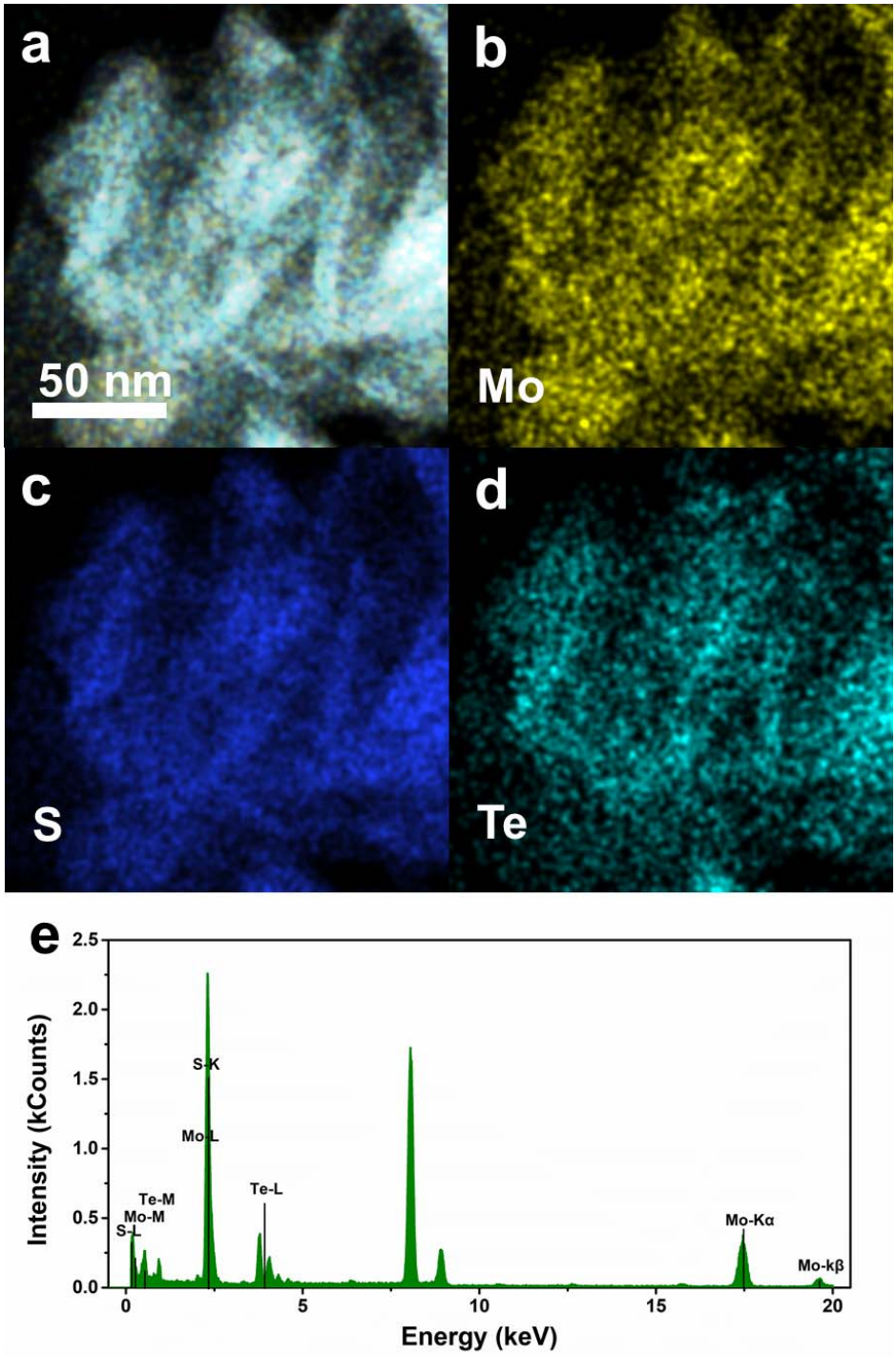

Figure S4. HAADF-STEM element mapping images of Te doped 1T@2H MoS_2: (a) integrated image, (b) Mo, (c) S, (d) Te and (e) EDX survey spectrum.

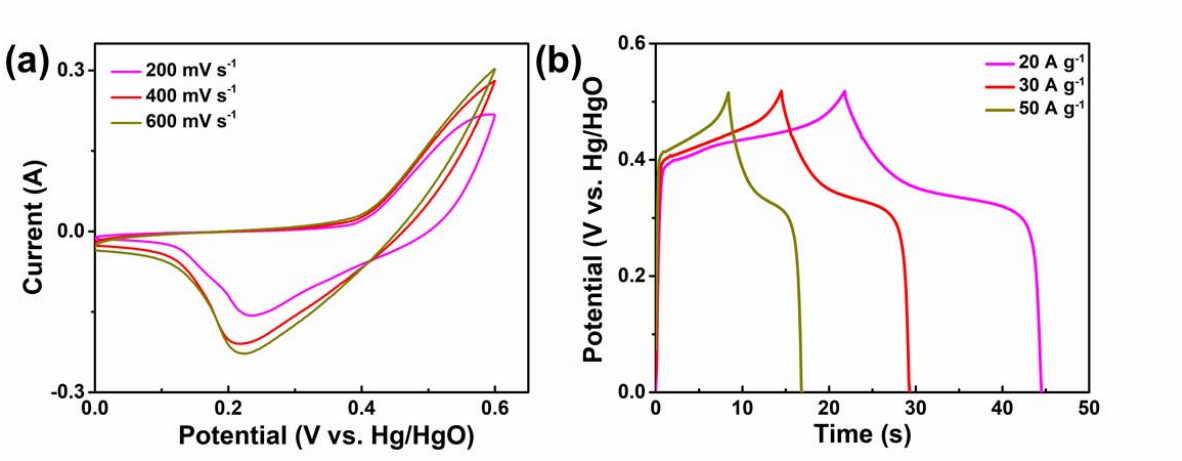

Figure S5. (a) CV curves of the Te doped1T@2H MoS_2 homojunction electrode at different scan rates; (b) GCD curves of the 1T@2H MoS_2 homojunction electrode at various current densities of 20, 30 and 50 A g^{-1}.

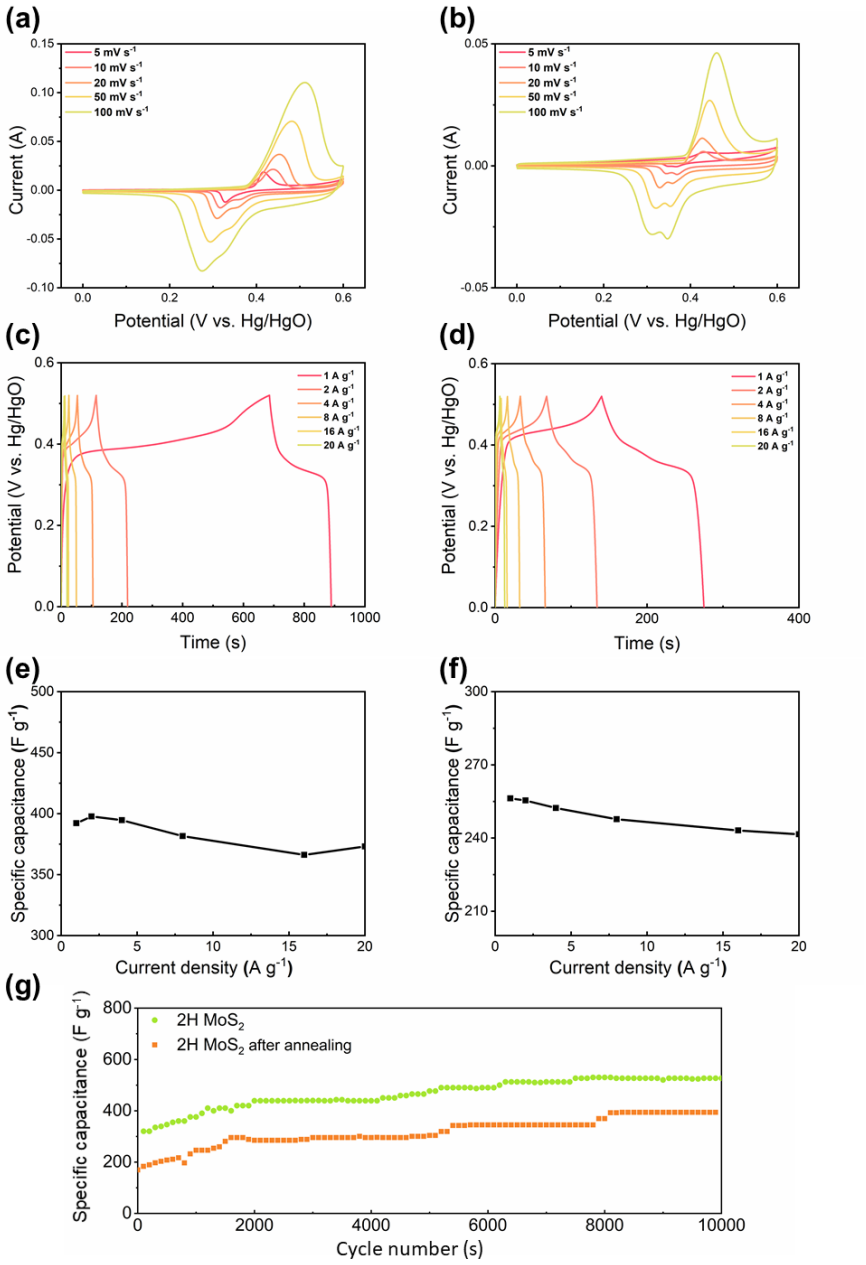

Figure S6. The electrochemical performance of the 2H-MoS_2 and 2H-MoS_2 after annealing electrode. (a) and (b) the CV curves at different scan rates of the 2H-MoS_2 and 2H-MoS_2 after annealing electrode; (c) and (d)galvanostatic charge-discharge curves at various current densities of the 2H-MoS_2 and 2H-MoS_2 after annealing electrode;(e) and (f) variations in specific capacitance with current density of the 2H-MoS_2 and 2H-MoS_2 after annealing electrode; (g) cycling performance of the 2H-MoS_2 and 2H-MoS_2 after annealing electrode after 10000 cycles at 10 A g^{-1}.

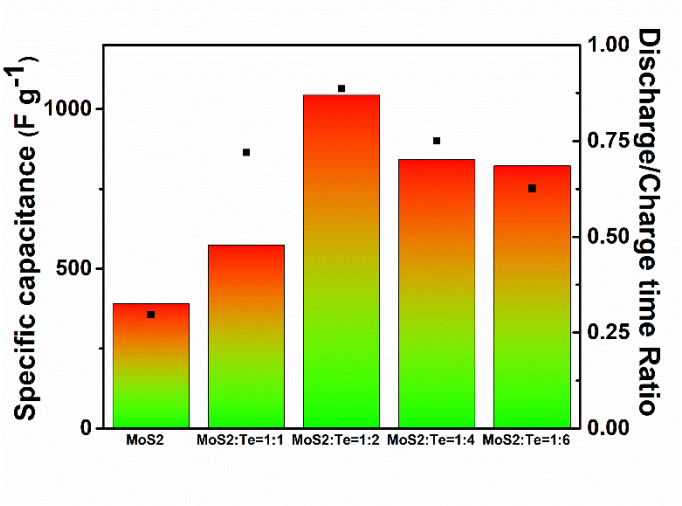

Figure S7. Specific capacitance and discharge/charge time of different ratio of Te doped 1T@2H MoS_2

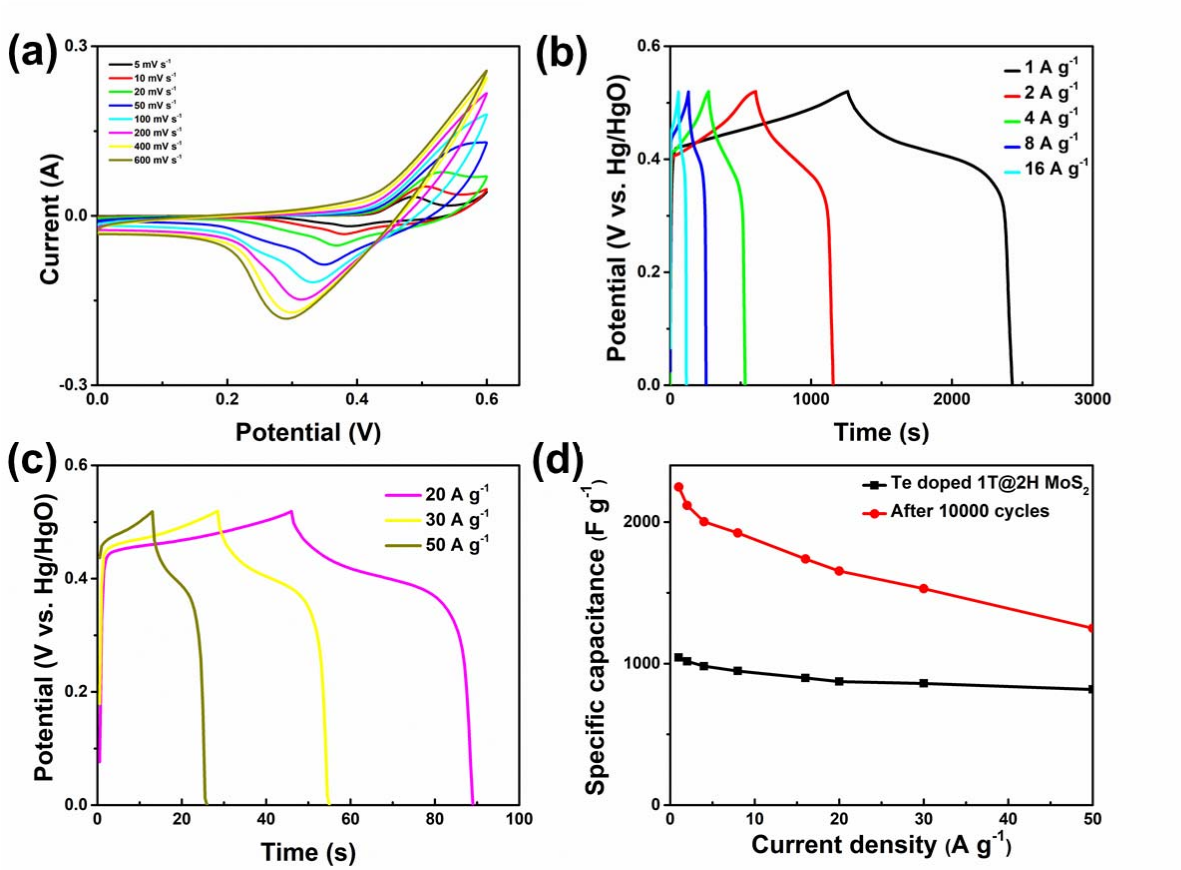

Figure S8. (a) CVs at different scan rates; (b) and (c) GCD curves at various current densities of Te doped 1T@2H MoS_2 electrode after 10000 cycles; (d) Variation in specific capacitance with current density for pristine homojunction and cycled one.

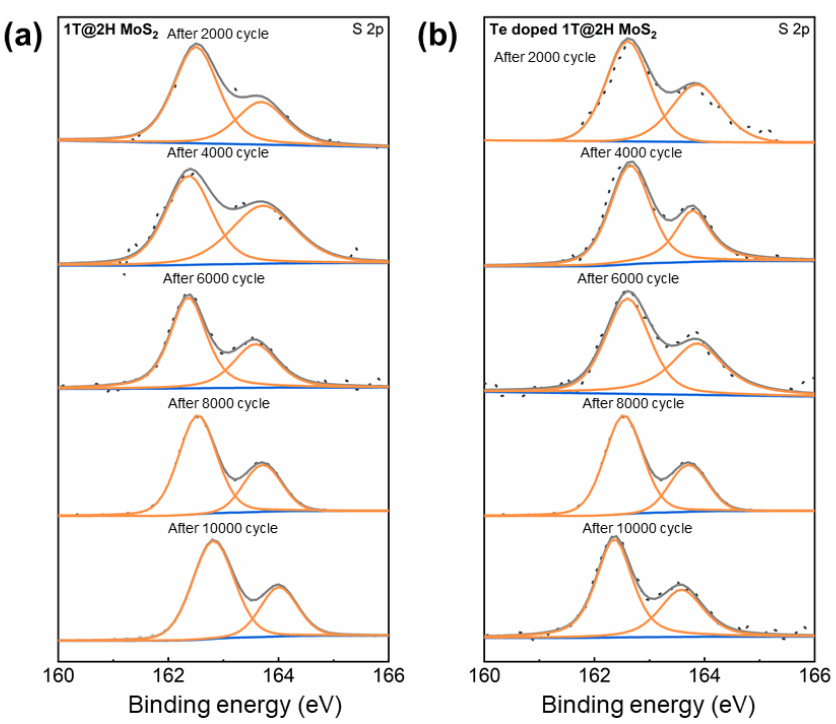

Figure S9. Ex-situ XPS of S 2p of (a) Initial 2H-MoS_2 after 2000 cycle and every 2000 electrochemical cycle 1T@2H MoS_2; (b) initial Te doped 1T@2H MoS_2 after 2000 cycle and every 2000 electrochemical cycle Te doped 1T@2H MoS_2.

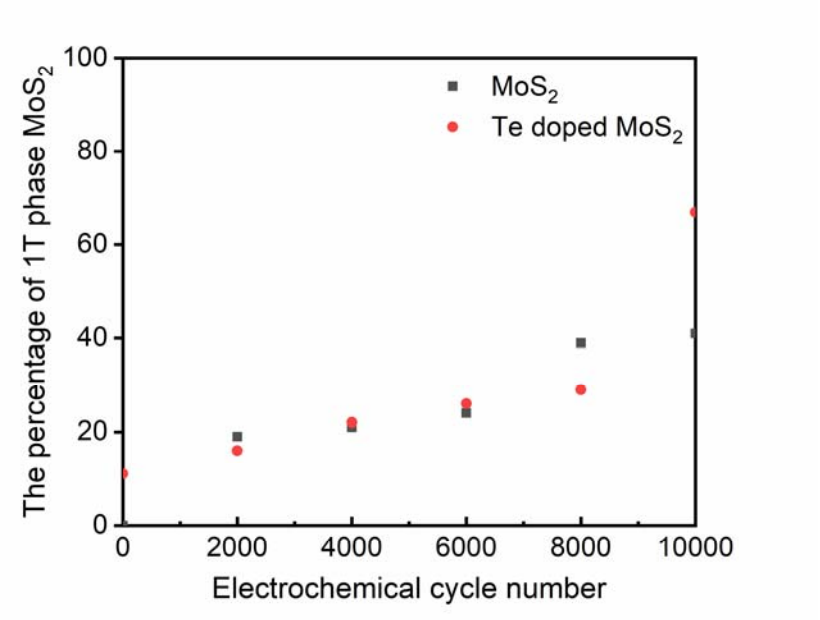

Figure S10. The dependent content change of 1T phase on the electrochemical cycles.

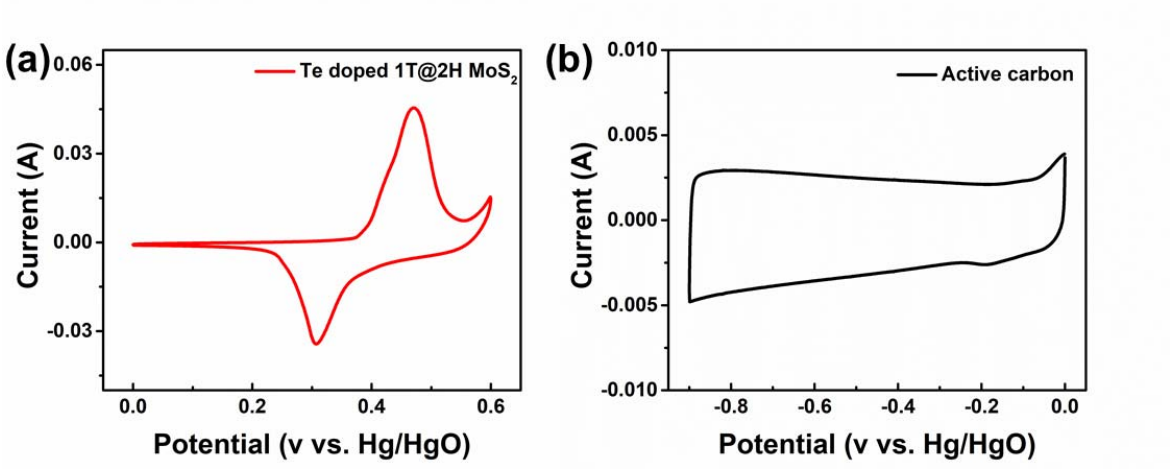

Figure S11. The CV curves of (a) Te doped 1T@2H MoS_2 and (b) AC.

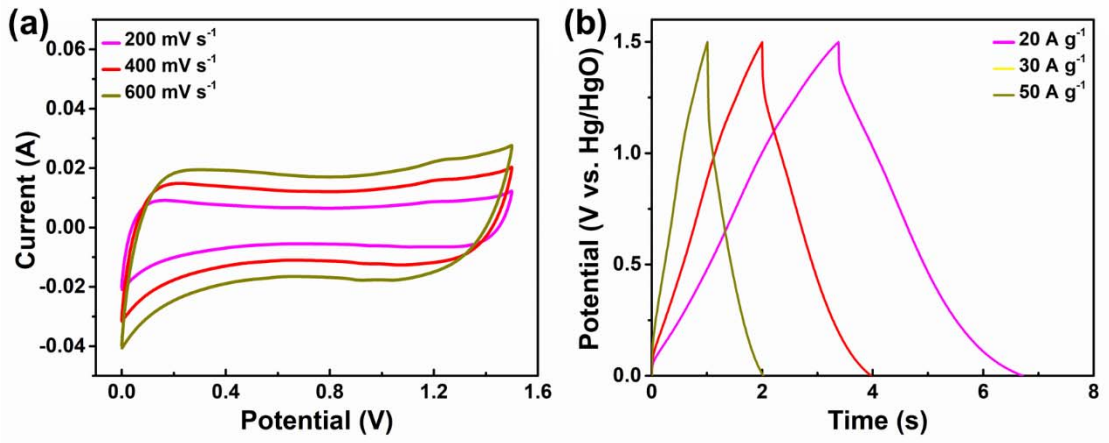

Figure S12. (a) CV curves at different scan rates and (b) GCD curves at various current densities of the ASC device.

Table S1. Summary of specific capacitances for MoS_2-based electrodes

Electrode materials	Specific capacitance (F/g)	Electrolyte	Voltage window (V)	Current load or scan rate	Refs
Te doped 1T@2H MoS_2	**1053.8 (origin) 2248 (improved)**	2M KOH	-0.25- 0.55 (AgCl/Ag)	1 A/g	This work
MoS_2-H_2O	**380**	0.5M Li_2SO_4	-0.25- 0.55 (AgCl/Ag)	5 mV/s	[9]
MoS_2/PANI	**552**	1M H_2SO_4	-0.1- 0.6(AgCl/Ag)	0.5 A/g	[10]
1T/2H MoS_2	**346**	2M KOH	0- 0.5(SCE)	1 A/g	[11]
Ni_3S_4–MoS_2	**985.21**	3M KOH	0- 0.53V(Hg/HgO)	1 A/g	[12]
MoS_2/PANI-38	**390**	H_2SO_4	-0.2- 1.0 V	0.8 A/g	[13]
a-MoS_x	**463**	1M Na_2SO_4	-1.0- -0.3 V	1 A/g	[14]
YS-MoS_2	**343**	1M Na_2SO_4	-1.0- -0.2 V	0.25 A/g	[15]
PANI/MoS_2	**575**	1M H_2SO_4	-0.4- 0.6 V (Hg/HgO)	1 A/g	[16]
MoS_2-graphene	**243**	1M Na_2SO_4	-1.0- 0 V (Hg/HgO)	1 A/g	[17]
PPy/MoS_2	**553.7**	1M KCl	-0.5- 0.3 V (SCE)	1 A/g	[18]
mesoporous MoS_2	**403**	1M KCl	-0.3- 0.5 V (SCE)	1 mV/s	[19]
1T/2H MoS_2	**366.9**	6M KOH	-0.1- 0.5 V (SCE)	0.5 A/g	[20]
Cu-doped MoS_2	**502**	1M Na_2SO_4	-0.35- 0.3(AgCl/Ag)	1 A/g	[21]

Table S2. Crystallographic Information Files (CIF) of each model over various 1T@2H ratios.

The content of 1T phase	MoS_2	Te doped MoS_2
16%	CIF-1	CIF-Te-1
32%	CIF-2	CIF-Te-2
50%	CIF-3	CIF-Te-3
66%	CIF-4	CIF-Te-4
83%	CIF-5	CIF-Te-5

Refs.

1. Perdew, J. P.; Burke, K.; Ernzerhof, M. Generalized gradient approximation made simple. *Phys. Rev. Lett.* **1996,** *77* (18), 3865.

2. Delley, B. An all-electron numerical method for solving the local density functional for polyatomic molecules. *J. Chem. Phys.* **1990,** *92* (1), 508-517.

3. Delley, B. From molecules to solids with the DMol3 approach. *J. Chem. Phys.* **2000,** *113* (18), 7756-7764.

4. Perdew, J. P.; Burke, K.; Ernzerhof, M., Generalized Gradient Approximation Made Simple. *Phys. Rev. Lett.* **1996,** *77* (18), 3865-3868.

5. Delley, B., An all-electron numerical method for solving the local density functional for polyatomic molecules. *J. Chem. Phys.* **1990,** *92* (1), 508-517.

6. Delley, B., From molecules to solids with the DMol3 approach. *J. Chem. Phys.* **2000,** *113* (18), 7756-7764.

7. Lu, T.; Chen, F., Multiwfn: A multifunctional wavefunction analyzer. *J. Comput. Chem.* **2012,** *33* (5), 580-592.

8. Gaussian 09, Revision D.01, M. J. Frisch, G. W. Trucks, H. B. Schlegel, G. E. Scuseria, M. A. Robb, J. R. Cheeseman, G. Scalmani, V. Barone, B. Mennucci, G. A. Petersson, H. Nakatsuji, M. Caricato, X. Li, H. P. Hratchian, A. F. Izmaylov, J. Bloino, G. Zheng, J. L. Sonnenberg, M. Hada, M. Ehara, K. Toyota, R. Fukuda, J. Hasegawa, M. Ishida, T. Nakajima, Y. Honda, O. Kitao, H. Nakai, T. Vreven, J. A. Montgomery, Jr., J. E. Peralta, F. Ogliaro, M. Bearpark, J. J. Heyd, E. Brothers, K. N. Kudin, V. N. Staroverov, T. Keith, R. Kobayashi, J. Normand, K. Raghavachari, A. Rendell, J. C. Burant, S. S. Iyengar, J. Tomasi, M. Cossi, N. Rega, J. M. Millam, M. Klene, J. E. Knox, J. B. Cross, V. Bakken, C. Adamo, J. Jaramillo, R. Gomperts, R. E. Stratmann, O. Yazyev, A. J. Austin, R. Cammi, C. Pomelli, J. W. Ochterski, R. L. Martin, K. Morokuma, V. G. Zakrzewski, G. A. Voth, P. Salvador, J. J. Dannenberg, S. Dapprich, A. D. Daniels, O. Farkas, J. B. Foresman, J. V. Ortiz, J. Cioslowski, and D. J. Fox, Gaussian, Inc., Wallingford CT, 2013.

9. Geng, X.; Zhang, Y.; Han, Y.; Li, J.; Yang, L.; Benamara, M.; Chen, L.; Zhu, H. Two-Dimensional Water-Coupled Metallic MoS_2 with Nanochannels for Ultrafast Supercapacitors. *Nano Lett.* **2017,** *17* (3), 1825-1832.

10. Ren, L.; Zhang, G.; Yan, Z.; Kang, L.; Xu, H.; Shi, F.; Lei, Z.; Liu, Z.-H. Three-Dimensional Tubular MoS_2/PANI Hybrid Electrode for High Rate Performance Supercapacitor. *ACS Appl. Mater. Interfaces* **2015,** *7* (51), 28294-28302.

11. Wang, D.; Xiao, Y.; Luo, X.; Wu, Z.; Wang, Y.-J.; Fang, B. Swollen Ammoniated MoS_2 with 1T/2H Hybrid Phases for High-Rate Electrochemical Energy Storage. *ACS Sustainable Chem. Eng.* **2017,** *5* (3), 2509-2515.
12. Luo, W.; Zhang, G.; Cui, Y.; Sun, Y.; Qin, Q.; Zhang, J.; Zheng, W. One-step extended strategy for the ionic liquid-assisted synthesis of Ni_3S_4–MoS_2 heterojunction electrodes for supercapacitors. *J. Mater. Chem. A* **2017,** *5* (22), 11278-11285.
13. Wang, J.; Wu, Z.; Hu, K.; Chen, X.; Yin, H. High conductivity graphene-like MoS_2 /polyaniline nanocomposites and its application in supercapacitor. *J. Alloys Compd.* **2015,** *619*, 38-43.
14. Shang, M.; Du, C.; Huang, H.; Mao, J.; Liu, P.; Song, W. Direct electrochemical growth of amorphous molybdenum sulfide nanosheets on Ni foam for high-performance supercapacitors. *J. Colloid Interface Sci.* **2018,** *532*, 24-31.
15. Wang, P.; Zhou, C.; Zheng, B.; Liu, H.; Sun, S.; Guo, D. Synthesis of yolk–shell MoS_2 microspheres with enhanced supercapacitance. *Mater. Lett.* **2018,** *233*, 286-289.
16. Huang, K.-J.; Wang, L.; Liu, Y.-J.; Wang, H.-B.; Liu, Y.-M.; Wang, L.-L. Synthesis of polyaniline/2-dimensional graphene analog MoS_2 composites for high-performance supercapacitor. *Electrochim. Acta* **2013,** *109*, 587-594.
17. Huang, K.-J.; Wang, L.; Liu, Y.-J.; Liu, Y.-M.; Wang, H.-B.; Gan, T.; Wang, L.-L. Layered MoS_2–graphene composites for supercapacitor applications with enhanced capacitive performance. *Int. J. Hydrogen Energy* **2013,** *38* (32), 14027-14034.
18. Ma, G.; Peng, H.; Mu, J.; Huang, H.; Zhou, X.; Lei, Z. In situ intercalative polymerization of pyrrole in graphene analogue of MoS_2 as advanced electrode material in supercapacitor. *J. Power Sources* **2013,** *229*, 72-78.
19. Ramadoss, A.; Kim, T.; Kim, G.-S.; Kim, S. J. Enhanced activity of a hydrothermally synthesized mesoporous MoS_2 nanostructure for high performance supercapacitor applications. *New J. Chem.* **2014,** *38* (6), 2379-2385.
20. Jiang, L.; Zhang, S.; Kulinich, S. A.; Song, X.; Zhu, J.; Wang, X.; Zeng, H. Optimizing Hybridization of 1T and 2H Phases in MoS_2 Monolayers to Improve Capacitances of Supercapacitors. *Mater. Res. Lett.* **2015,** *3* (4), 177-183.
21. Falola, B. D.; Fan, L.; Wiltowski, T.; Suni, I. I. Electrodeposition of Cu-Doped MoS_2 for Charge Storage in Electrochemical Supercapacitors. *J. Electrochem. Soc.* **2017,** *164* (9), D674-D679.